

A Novel Fusion Method for Soybean Yield Prediction Using Sentinel-2 and PlanetScope Imagery

Khilola Amankulova , Nizom Farmonov , Enas Abdelsamei , József Szatmári , Waleed Khan , Mohamed Zhran , Jamshid Rustamov, Sharifboy Akhmedov, Maksudxon Sarimsakov, and László Mucsi 

Abstract—This study aimed to develop a new method for combining Sentinel-2 and PlanetScope (PS) imagery. The normalized difference vegetation indices (NDVI) data were retrieved from the Earth observation satellites S2 Level-2A and PS Level-3 surface reflectance during the soybean growing phase. The proposed method utilizes the Python implementation of data mining sharpener algorithm, which is a decision-tree-based technique for enhancing low- and high-resolution images with information from large-scale images. The robustness and flexibility of a multidimensional data fusion, deep neural network, and machine-learning-based yield estimation model were analyzed based on the within-field variability in soybean yield. A comparative analysis revealed that the fusion data with 1.5–2.5 tons significantly outperformed individual predictions, demonstrating higher accuracy and fewer errors. The fusion data used to predict yields showed relatively small error ranges of 0.5–0.2 t/ha. In contrast, the PS and S2 datasets showed higher prediction errors. The study employed vegetation indices, and during validation, crop forecasts were compared using an NDVI map. The effectiveness of artificial neural networks in predicting crop yields was highlighted, demonstrating superior performance across diverse datasets compared with other algorithms. This novel fusion technique is essential for monitoring crop health and growth, improving agricultural practices, such as fertilization and water management, and improving yield forecast accuracy. This study provides valuable insights into phenology monitoring, image fusion accuracy, and the effectiveness of machine-learning algorithms in predicting crop yields, emphasizing the benefits of fused imagery.

Manuscript received 9 January 2024; revised 16 April 2024; accepted 9 May 2024. Date of publication 16 May 2024; date of current version 9 August 2024. This work was supported in part by the University of Szeged Open access fund under Grant 7028. (*Corresponding author: Khilola Amankulova*.)

Khilola Amankulova, Nizom Farmonov, Enas Abdelsamei, József Szatmári, and László Mucsi are with the Department of Geoinformatics, Physical and Environmental Geography, University of Szeged, H-6722 Szeged, Hungary (e-mail: amankulova.khilola@stud.u-szeged.hu; farmonov.nizom@stud.u-szeged.hu; enas.mohammed@nriag.sci.cgi; szatmari.jozsef@szte.hu; mucsi@geo.u-szeged.hu).

Waleed Khan is with the Department of Computer Systems Engineering, University of Engineering and Technology Peshawar, Peshawar 25000, Pakistan, and also with the National Center for Big Data and Cloud Computing, Lahore 54000, Pakistan (e-mail: khanwaleed@uetpeshawar.edu.pk).

Mohamed Zhran is with the Public Works Engineering Department, Faculty of Engineering, Mansoura University, Mansoura 35516, Egypt (e-mail: mohamedzhran@mans.edu.eg).

Jamshid Rustamov is with the Department of Land Resources, Cadastre and Geoinformatics, Karshi Institute of Irrigation and Agrotechnology “TIIAME” National Research University, Karshi 100000, Uzbekistan (e-mail: rustamov-jamshid1985@gmail.com).

Sharifboy Akhmedov and Maksudxon Sarimsakov are with the Department of Hydrology and Ecology, “TIIAME” NRU Bukhara Institute of Natural Resources Management, Bukhara 200109, Uzbekistan (e-mail: ahmedovsarifboj652@gmail.com; ingengineering67@gmail.com).

Digital Object Identifier 10.1109/JSTARS.2024.3402114

Index Terms—Crop monitoring, data fusion, PlanetScope (PS), time series, vegetation indices (VIs).

I. INTRODUCTION

CROP productivity research has gained significant importance as a crucial benchmark for farm management throughout the agricultural cycle, encompassing planning, agrotechnological interventions, and pre- and postharvest processes [1]. Early yield forecasting at the field and farm levels, particularly in combination with the mapping of yield variations within the field, plays a crucial role in crop management. This enables precise site-specific decisions on fertilization, irrigation, and weed control [2], [3]. According to Wolfert et al. [4], the agricultural sector has witnessed a continuous increase in data-generating devices and sensors, empowering farmers to adopt data-driven decision-making approaches.

Soybeans are recognized for their high-quality animal feed and as a crucial protein source for global populations, with paramount significance [5]. The European Commission estimates that soybeans constitute a significant proportion of annual and perennial crops. In view of the projected increase in food demand by 2030, soybean production is expected to grow (EU Agricultural Outlook, accessed on 17 April 2020).

Due to its commendable macroperformance and periodic data availability [6], remote sensing has found extensive utility in agricultural applications, encompassing tasks, such as cropland cover classification, drought stress assessment, and yield estimation. The availability of high-quality, publicly accessible terrestrial data sources, such as Landsat-8 and Sentinel-2 (S2), has been widely used. Additionally, the emergence of a new generation of nanosatellites, exemplified by Planet Labs’ PlanetScope (PS) CubeSat constellation, has democratized high-resolution spatial and temporal data acquisition at a significantly reduced cost [7], [8, p. 201]. However, PS imagery is susceptible to cross-sensor discrepancies that introduce noise into the time series of observations derived from these sensors [9]. Addressing this challenge entails the integration of PS images with a consistent and dependable dataset, such as S2, offering a means to effectively mitigate noise in PS data [10].

As highlighted by Sun et al. [11], valuable external data can be harnessed from remote sensing sources in crop yield prediction. These sources often tap into the visible red, green, and blue segments of the electromagnetic spectrum and near-infrared (NIR) bands. These spectral components are essential in monitoring critical aspects of crop cultivation, including crop health, soil

moisture, nitrogen stress, and ultimately crop yields, as evidenced by the works of [12], [13], [14], [15], and [16]. Among these studies, vegetation indices (VIs), with the normalized difference VI (NDVI) at the forefront, have been widely used because of their effectiveness, as demonstrated by the authors in [15], [16], and [17]. Furthermore, additional indices, such as the soil-adjusted VI (SAVI) [18], enhanced VI (EVI) [19], green NDVI (GNDVI), and normalized difference red edge (NDRE) [20], have played crucial roles in estimating crop production.

Researchers commonly use regression or correlation analyses to establish the statistical connection between controlled variables and crop yield [21]. However, the widespread use of linear statistical models in current crop yield prediction is limited, particularly the nonlinear interactions within the data. Simple or multiple linear regression (MLR) models are the typical go-to options for predicting crop yield [22], [23]. It is worth noting that MLR analysis can be constrained when dealing with highly correlated input parameters, limiting the inclusion of only a few predictor variables [24]. Additionally, determining the most suitable algorithm for prediction can be challenging, even though advanced models, such as the XGBoost algorithm, are favored by many researchers due to their speed, efficiency, and minimal data requirements [25].

The accurate and reliable estimations of crop yields necessitate the use of high-quality remote sensing data and the implementation of sophisticated and automated technologies [26]. Deep learning (DL) models, particularly convolutional neural networks, have unequivocally demonstrated significant potential across a spectrum of critical remote sensing applications, including crop yield estimation [11], [27]. These DL models possess the intrinsic ability to autonomously discern features across various levels of statistical modeling, a marked departure from traditional regression methodologies that often mandate feature engineering and domain expertise for feature extraction from imagery [28].

Artificial neural networks (ANNs) take inspiration from the human learning process and adopt a fundamental architecture composed of interconnected nodes to construct classification models primarily based on the statistical data, reducing the need for task-specific, explicit rule-based programming [6]. DL models, or deep ANNs characterized by more than two hidden layers, offer a solution to the challenges posed by the curse of dimensionality, enabling them to construct classification models directly from data in an end-to-end fashion. This contrasts with the conventional approach of manual feature engineering, which relies on human intuition and prior experience [29].

A few endeavors to fuse PS imagery with S2 visual images into high spatiotemporal datasets were prompted by the lack of results of high spatial and temporal resolution time series from well-calibrated satellite images. For example, the moderate-resolution imaging spectroradiometer-Landsat SaTellite dAta IntegRation (STAIR) integration product and PS data were combined to generate daily leaf area index (LAI) assessments for corn and soybean in the United States Corn Belt [30]. The STAIR approach uses a resilient adjustment that reports for multiple land cover types via feature extraction [31], [32]. Soybean was estimated through RGB, multispectral, and thermal sensors using deep neural network (DNN) R^2 with an accuracy of 0.720

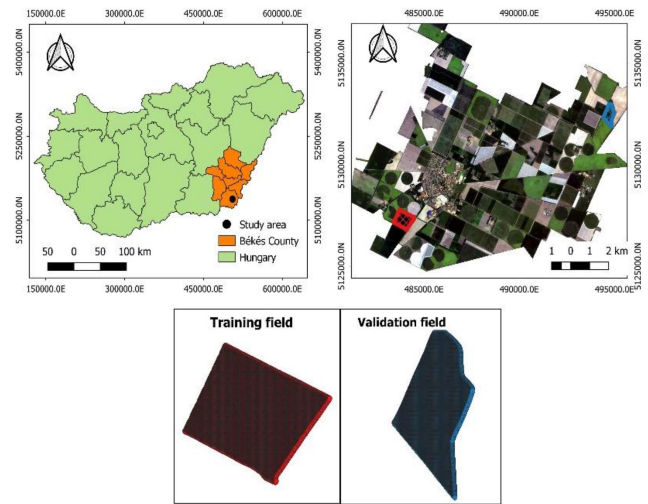


Fig. 1. Study area.

[32]. Additionally, soybean yield prediction was investigated using RS and crop yield at the field scale [33]. MLR models were developed based on the L8 and S2 NDVI at the soybean growth stages. It was discovered that soybean grain yield can be predicted between 29 and 46 days after planting, with a mean prediction error of 153.9 kg/ha. Previous research supports the individual capability of S2 and L8 for estimating soybean yield. However, the full potential of these sensors has yet to be realized. Most of these studies relied solely on RS data, limiting the applicability of these methods to other areas. Therefore, there is a need for more research and development to create a reliable model for predicting soybean yield.

The main objectives of this study are summarized as follows.

- 1) We use a time series and select the most substitute period to fuse two constellations.
- 2) PS images (spatial resolution of 3 m and daily revisit time) are fused with S2 images (spatial resolution of 10 m and five-day revisit time), and VIs are calculated for fusible images.
- 3) Based on the within-field variability of soybean yield, we analyze the robustness and flexibility of a multidimensional data fusion, DNN, and machine-learning (ML) based yield estimation model and compare all datasets.

II. MATERIALS AND METHODS

A. Study Area

The study parcel is in Mezhegyes town, Békés county, southeast Hungary, near the Romanian border (latitude 46°19'N, longitude 20°49'E), near the Mezhegyes experimental farm (see Fig. 1). The town has 4950 residents and a total administrative area of 15 544 ha. For our research, we utilized two plots: the first plot, serving as the training site, covered an area of 78 ha, while the second plot, designated for validation purposes, covered 37 ha. Soybean is the most widely grown crop with a total of 1090 ha. Chernozem is a popular type of soil that promotes plant development and produces abundant crops. Meadow and lowland chernozem are excellent foundations for field cultivation

because of their high lime content. The fertile soil of chernozem, which is best suited for cultivating crops, particularly cereals and oilseeds, provides high agricultural yields and excellent agronomic conditions. Mezhegyes' experimental farm, Mezhegyesi Ménésbirtok Zrt., has a significant impact on Mezhegyes and surrounding communities. In 2021, the average annual rainfall was 645 mm (428.9 mm for crops). In the study area, the average annual temperatures range from 7.8 to 11.1 °C.

B. Field Data Collection

The high-resolution soybean yield data were collected using a combined machine equipped with a yield monitoring system and GPS between 7 and 18 October 2021, harvesting season. Soybean yield crops in Hungary are usually planted in April and harvested in September. Raw yield data were cleaned to remove inaccurate grain yield measurements caused by the harvesting dynamics of the combine harvester and the precision of the positioning data [34]. Commercial yield monitors will likely produce inaccurate data when harvested rows overlap, indicating a poor crop yield in certain parts of the field. Therefore, straight-line sequences of locations with yields near zero were eliminated. The company that owns and operates farms in the study area calibrated and filtered the crop yield data. Only crop yield data with the same width and length as the header dimensions of the combined harvester (i.e., 2 m × 6 m) remained. To match the resolution of the satellite images, we converted the crop yield data to raster format using QGIS v.3.16s inverse distance weighted interpolation method at 3-, 10-, and 30-m resolutions.

C. Imagery

1) *S2 Image Processing*: The European Space Agency Copernicus S2 contains a constellation of two polar-orbiting satellites arranged in the same sun-synchronous orbit but phased at 180° to each other. S2 is equipped with an optical sensor payload that samples 13 spectral bands: four, six, and three at 10, 20, and 60 m spatial resolution, respectively. A Level-2A (L2A) product provides images of the bottom of the atmosphere reflectance covering the visible and NIR spectral range derived from associated Level-1C datasets. MSIs are equipped on S2 A and B, allowing agricultural monitoring on regional and global scales at various spatial resolutions [35]. We downloaded 18 cloud-free S2 L2A satellite images during the study period.

2) *PS Image Processing*: PS super dove (PSB.SD), a new generation of DOVE CubeSat, was used in this study. The PSB.SD instrument has eight spectral bands (red edge, red, green, green I, yellow, blue, coastal blue, and NIR) and a pixel size of 3 m. The PS orthorectified product was geometrically and radiometrically corrected for surface reflection before being projected onto a UTM/WGS84 cartographic map (Planet Team, 2017). These images were harmonized with S2 for consistent radiometry. A total of 81 available cloud-free PS Level-3 surface reflectance products collected during the soybean growing phase between April and October were downloaded from the Planet Explorer website¹ (accessed on 25 August 2022).

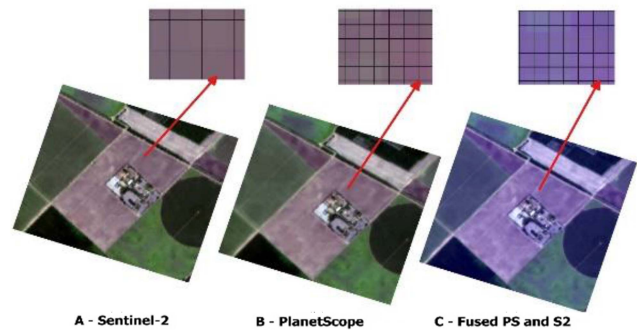


Fig. 2. Sample of the training site's S2 and PS fusion results. Image from (a) S2(10), (b) PS(3), and (c) fused (3 m).

D. Data Fusion

Although S2 satellite imagery has been widely used for yield prediction or vegetation detection, we decided to test a fusion of S2 imagery with PS because of its higher spatial resolution. The primary goal of this study is to develop a new method for combining S2 and PS imagery. The PS + S2 method introduces geometry information from the higher resolution image by aligning all edges of the higher resolution image with each lower resolution multispectral band. The method assumes that images taken in different spectral bands share common geometric information and that the higher resolution image can be approximated as a linear combination of the high-resolution multispectral bands to obtain the spectral information for the fused image. Each S2 band was first fused with a high-resolution PS band with similar spectral properties (see Fig. 2).

As a novel approach, we developed an automated fusion method using the Python implementation of data mining sharpener (pyDMS) algorithm, which is a decision-tree-based technique for enhancing low-resolution images with information from high-resolution images [36]. The input data for this method consist of high-resolution PS images with a spatial resolution of 3 m and shortwave reflectance data.

Data Preparation: Data preparation involves several key steps, including aggregation and calibration. Aggregation refers to the process of combining low-resolution and high-resolution bands to match the spatial resolution of PS imagery. Calibration ensures that the data are adjusted and interpreted correctly to maintain accuracy and consistency throughout the fusion process.

Homogeneity Check: To ensure the effectiveness of the fusion process, a homogeneity check is conducted to assess the level of consistency between high-resolution and low-resolution pixels. This step aims to identify and exclude any sources of noise or interference that may affect the quality of the fused imagery.

Fusion Process: The pyDMS algorithm employs an ensemble of decision-tree regressors, utilizing the bagging technique, which involves creating multiple subsets of the original dataset through random sampling with replacement [37]. Each decision tree, also known as an RF, is trained on a bootstrap sample, and the final result is a combination of the predictions from individual trees. This ensemble approach enhances the robustness

¹[Online]. Available: <https://www.planet.com/explorer/>

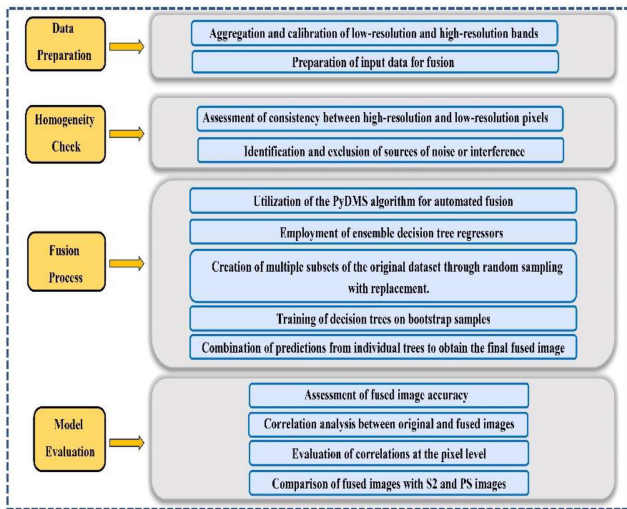


Fig. 3. Flowchart of the image fusion.

TABLE I
MULTISPECTRAL VIs WERE INVESTIGATED IN THIS STUDY

Index	Equation	Reference
NDVI	$\frac{NIR - Red}{NIR + Red}$	[38]
GNDVI	$\frac{NIR - Green}{NIR + Green}$	[39]
NDRE	$\frac{NIR - Red Edge}{NIR + Red Edge}$	[40]
EVI	$2.5 \frac{NIR - Red}{(NIR + 6Red - 7.5Blue) + 1}$	[41]
SAVI	$(1 + L) \frac{(NIR - Red)}{(NIR + Red + L)}$	[42]

and accuracy of the fusion process, enabling the generation of high-quality fused images from PS and S2 data.

By incorporating the pyDMS algorithm and employing a rigorous fusion process, we ensure the production of high-quality fused imagery that enhances the accuracy and reliability of soybean yield prediction models.

1) *Local and Global Regression*: The ensemble decision tree is performed locally (through a moving window) and globally (entire study area). These results are combined based on the regression outputs and low-resolution data. The pyDMS application uses an ensemble of decision-tree regressors, employing a bagging technique that creates multiple subsets of the original dataset through random sampling with replacement. These processes are presented in Fig. 3.

E. Fused VIs

We calculated five VIs for the new fuse dataset, as well as the original S2 and PS images (see Table I). NDVI [38] and GNDVI [43] are well established and can easily retrieve spectral reflectance indicators of crop heat stimuli [44], [45],

TABLE II
CORRELATION (R^2) AMONG S2, PS, AND THE FUSED IMAGES OF ALL THE IMAGES ANALYZED FOR EACH BAND AND ALL FIVE BANDS

Satellite datas	Blue	Green	Red	Red edge	NIR	All
PS_S2	0.88	0.92	0.95	0.85	0.96	0.95
Fused_PS	0.91	0.94	0.96	0.86	0.88	0.89
Fused_S2	0.96	0.96	0.98	0.96	0.88	0.9

[46], [47], [48]. GNDVI was developed by Gitelson et al. [39] to address saturation issues observed with NDVI for some vegetation types at later growth stages. However, Thompson et al. [40] demonstrated that red-edge bands based on NDRE could effectively identify crop populations with a higher correlation using indicators, such as plant nitrogen accumulation, to address the saturation resolution problem. GNDVI is more useful for assessing leaf chlorophyll variability when LAI is relatively high because it uses the green band instead of the red band in the NDVI estimator [39]. Gianelle et al. [49] recognized that GNDVI was less affected by saturation and produced consistent results for various leading indicators of vegetation effectiveness. EVI reduces soil background and atmospheric factors that influence reflectance data by including reflectance in the blue band of the electromagnetic spectrum in addition to the red and NIR bands [41]. Meanwhile, SAVI includes a soil adjustment factor to compensate for the difference in soil brightness influence. This factor ranges from 0 to 1 depending on the amount of visible soil. Maximum levels should be used in areas with more visible bare soil [50].

Crop phenology is dynamic during the growing season [51]. Farmers and researchers conducted bimonthly phenological observations and recorded transition dates throughout the soybean growing season. These observations were made for all soybean plots. They also compared the spectral reflectance patterns obtained from satellite data with the on-ground field observations. In QGIS 3.16s polygon tool, points were obtained using the random point feature. To determine the crop phenology and transition dates, NDVI values were retrieved from the soybean fields using QGIS' point sample tool and open-source plugin. Phenological phases for soybeans were created by averaging and distributing the 65 NDVI points randomly generated in soybean field boundaries using QGIS (Fig. 4).

F. Phenology Monitoring

In this study, we employed the phenological stages from the NDVI data obtained from PS and S2 satellites. The spatial resolution of the NDVI data was significantly improved using this approach. This enhanced dataset facilitates the precise determination of soybean phenological periods. Identifying the growth

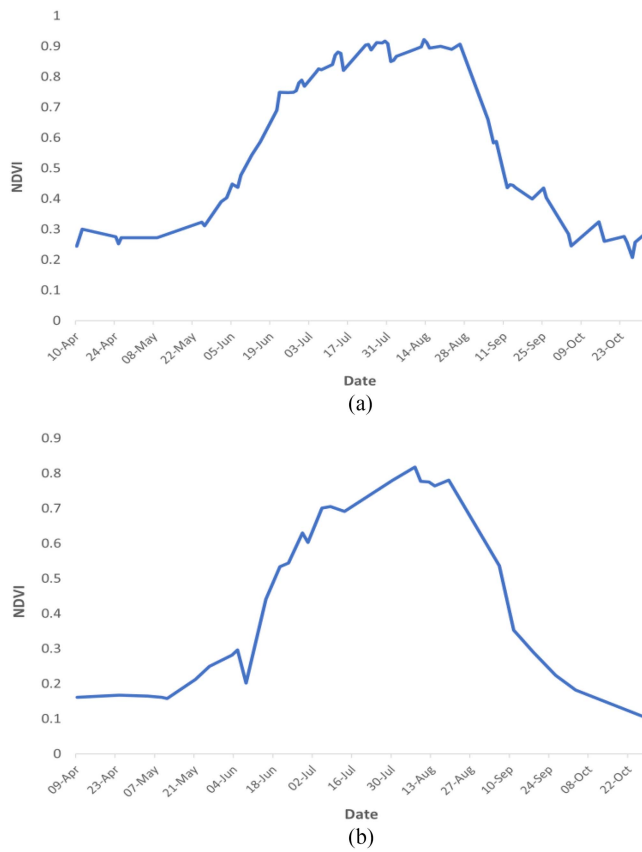


Fig. 4. Soybean phenological stages based on (a) S2 and (b) PS NDVI during the growing season.

stage with the most substantial impact on potential yield is instrumental in optimizing agricultural management practices [52]. For example, understanding how yield is influenced by specific growth stages, such as fertilization or pesticide application, as well as responses to stressors, such as cold weather, hail, low soil moisture, and plant diseases, can guide effective management strategies. Fig. 2 illustrates distinct temporal patterns extracted from satellite data. Notably, NDVI derived from PS and S2 data displayed nearly identical and consistent temporal patterns. The graph depicts initial lower values during the early vegetative period, followed by a steady increase, signifying the onset of vegetative stages, including leaf development and robust growth.

G. Fused Image Accuracy

We selected the date of 7th August based on the vegetation characteristics and combined the spectral mapping and correlation between PS and S2 satellite data to align their spectral profiles for subsequent band-to-band fusion. Table I illustrates the appearance of the chosen area in its original PS and S2 constellations, along with the fused image. The spectral properties of the acquired 3-m simulated image closely resemble the corresponding S2 bands, even though they exhibit some variability. Moreover, the simulated image is more than just a spectral data source, as demonstrated by Liu et al. [53]. This is because it has a real 3-m spatial resolution in every band,

making it an essential source of spatial information for further fusion processes.

We buffered the yield data to be 15 m from the field boundaries to reduce any edge effects related to mixed pixels. Processing and utilization were made easier by organizing the data into attribute tables, especially when combined into a point vector file. We conducted the processing using QGIS 3.16.

Correlations among S2, PS, and the fused images were evaluated at the pixel level. The correlation between PS and S2 was notably the highest in the NIR wavelength, reaching 0.96 for PS-S2 and 0.88 for fused_PS and fused_S2. The red-edge wavelength showed the lowest correlation, measuring 0.85. Across all five bands, the fused images exhibited significant correlations with the PS-S2 images, surpassing the correlations between the fused_PS and fused_S2 images, as presented in Table II.

H. ML Algorithms

ML is a subset of artificial intelligence and computer science dedicated to leveraging data and algorithms to emulate human learning processes, aiming to enhance accuracy through continuous improvement. It plays a pivotal role in the rapidly advancing field of data science. Through the application of statistical techniques, algorithms are trained to make classifications or predictions, unveiling valuable insights in data mining endeavors. Subsequently, these insights inform decision-making processes within various applications and enterprises [54].

1) *Random Forest Regression (RFR)*: RFR is an ML technique based on the decision-tree algorithm and is commonly used to forecast crop yields [55]. The RFR model creates a collection of tree predictors, each associated with distinct randomly chosen feature vectors. These trees, called decision trees, are developed with an emphasis on decorrelation during training. The final prediction from the RFR model is derived by averaging the output values from all these individual trees. In the RFR model, the learner bagging algorithm is employed to train each individual tree [37]. RFR is widely recognized for its exceptional accuracy, capability to handle large datasets with higher levels of complexity, and ability to handle missing data points. It also has great application in feature selection, which is evident from its feature importance rankings [56].

2) *K-Nearest Neighbors (KNNs)*: KNN is an ML technique used for regression and classification tasks. It relies on distance metrics, such as Manhattan or Euclidean, to estimate the target value for new data points by considering the k nearest neighbors. In this study, we used the Euclidean distance formula (1) to determine the distances between data points. The choice of k significantly impacts the prediction; a small value of k leads to high variability and low bias, whereas a large value of k leads to reduced variability and higher bias. The key advantage of KNN is its lack of training phase or optimization requirements. However, it has the limitation of high computational complexity and time consumption due to its dependence on historical data to make predictions for new observations [57]

$$d(p, q) = \sqrt{\sum_{i=1}^n (q_i - p_i)^2} \quad (1)$$

where d represents the Euclidean distance, which measures the distance between two points in space; p and q represent the data points, and they can have multiple dimensions; n denotes the total number of data points in a dataset, and i denotes an index number used to refer to a specific data point within the dataset.

3) *Support Vector Regression (SVR)*: In a high-dimensional feature space, SVR creates a linear regression model by transforming the data using a nonlinear function. This process helps improve the model's ability to capture complex relationships within the data [58].

4) *XGBoost*: XGBoost is an ML model commonly used to predict stock market trends over time [59]. It employs a group of decision trees and uses a gradient descent algorithm to create subsequent trees. This algorithm minimizes the loss function associated with the previous tree to improve the overall predictive performance [60]. XGBoost accelerates tree training through parallelization, significantly improving the training speed. This feature has found extensive application in tasks, such as predicting crop yields [61], [62], [63].

III. DEEP LEARNING

DL is an ML technique that draws inspiration from the architecture of the human brain [64]. It involves the process of training neural networks consisting of numerous layers. In DL, data representation is acquired at diverse levels of abstraction through multiple layers. The ability to learn complex functions is facilitated by employing DL with abundant data and numerous layers, each capturing features at different levels of abstraction [29].

A. Deep Neural Networks

DNN refers to a densely connected layer with a more significant number of layers in the network structure, allowing it to create more powerful and complex nonlinear representations. This advancement in network depth can effectively enhance the model's capabilities [65]. DNN models are effectively trained using gradient-based optimization techniques to minimize the specific loss function relevant to their intended task. These DNN models have demonstrated remarkable achievements, surpassing traditional ML approaches, in accurately predicting crop yields [28], [66], [67].

B. Artificial Neural Network

A three-layer ANN is employed to model and capture the complex, nonlinear relationships between the yield and various input features [68]. Information is gathered by neural networks through the identification of connections in data. Initially, the raw data are taken in by the first layer, undergoes processing, and relays to a hidden layer. Subsequently, the information is transmitted from the hidden layer to the final layer to generate the output [69].

C. Model Evaluation

Various common metrics are used to assess the performance of predictive models, including R -squared (R^2), root-mean-square

error (RMSE), mean absolute error (MAE), and mean absolute percentage error (MAPE). These metrics are widely used to evaluate the prediction performance of a model. The equations that describe the derivatives of these metrics are provided in [2], [3], [4], and [5]

$$R^2 = \left\{ \frac{1}{N} * \frac{\sum (X_i - \bar{X}) * (Y_i - \bar{Y})}{(\sigma_X - \sigma_Y)^2} \right\}^2 \quad (2)$$

$$\text{RMSE} = \sqrt{\frac{\sum_{i=0}^n |A_i - P_i|^2}{n}} \quad (3)$$

$$\text{MAE} = \frac{1}{N} \sum_{i=1}^N |Y_i - \bar{Y}| \quad (4)$$

$$\text{MAPE} = \frac{1}{N} \sum_{i=1}^N \left| \frac{Y_i - \bar{Y}}{Y_i} \right| * 100 \quad (5)$$

where A_i and P_i represent the measured and predicted values, respectively; N denotes the number of observations; X_i and Y_i are the X and Y values of observation i , respectively; \bar{X} and \bar{Y} are the mean X and Y , respectively; σ_x and σ_y are the standard deviations of X and Y , respectively; and S_i represents an intertemporal variance.

IV. RESULTS

A. Determine Peak Phenology Date

We used the NDVI data obtained from the PS and S2 sensors during the growth season to determine the peak phenological stage. Additionally, we used the smoothing spline method to improve the clarity of identifying the ideal time. The beginning of the growth season produced the lowest values in the NDVI values from both sensors. Consequently, an ongoing rise in NDVI was observed between 18 May and 12 June, indicating the start of vegetative phases, including cotyledon emergence and a significant increase in soybeans. In late July and early August, from 31 July to 8 August, soybean growth peaked, which is consistent with the highest NDVI values (see Fig. 2). Soybeans reached the early seed and seed stages when the NDVI started to decrease in late August. The lowest NDVI levels were observed during the September harvest season when the soybeans were fully mature.

B. Crop Yield Prediction With ML and DL Algorithms

In this study, we selected a single training field using PS, S2, and fusion imagery with VIs to facilitate crop yield prediction. This training field was subsequently partitioned into an 80/20 split to evaluate the prediction techniques. The effectiveness of these methods was assessed through the implementation of ML and DL algorithms. We comprehensively analyzed various evaluation metrics, including R^2 , RMSE, MAE, and MAPE, to assess the performance of different algorithms on the dataset. Subsequently, we compared the results obtained from these metrics to determine which algorithm yielded the most favorable

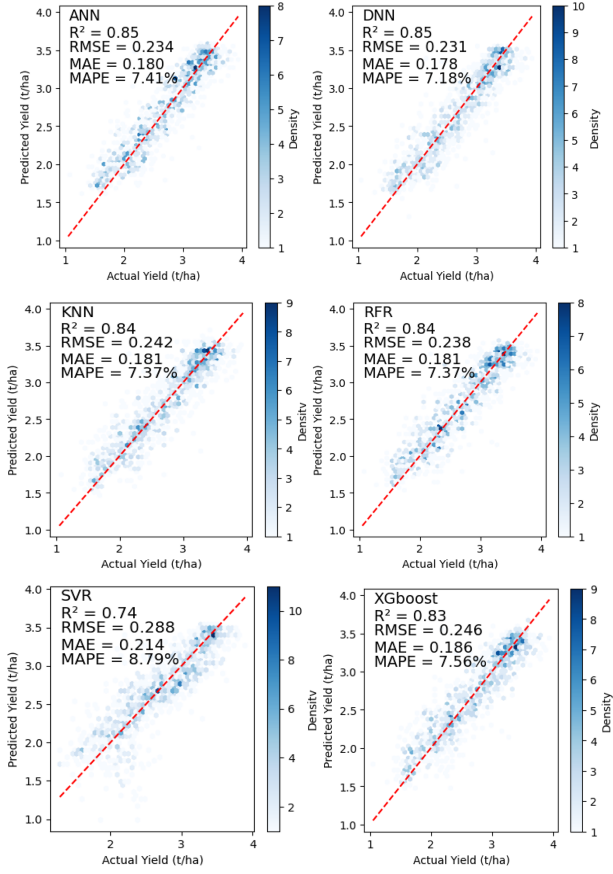


Fig. 5. Scatter plots comparing actual and predicted yields for training data, employing S2 and VIs with ANN, DNN, KNN, RFR, SVR, and XGBoost.

outcomes. We also generated scatter plots for each of the three datasets to provide a visual representation for the comparative analysis of the algorithms. This comprehensive analysis allowed us to identify the algorithm that exhibited superior performance across the evaluated datasets (see Figs. 5–7).

By comparing the scatter plots generated from the three datasets, we observed that the highest values were associated with the fusion dataset, followed by the PS and S2 datasets. Specifically, R^2 was 0.86 for the fusion dataset when analyzed using ANN, whereas it was 0.86 and 0.85 for the PS and S2 datasets, respectively. Additionally, when RMSE, MAE, and MAPE were used, the fusion dataset yielded values of 0.215 t/ha, 0.160 t/ha, and 6.49%, respectively (see Fig. 7). Comparatively, the PS dataset yielded values of 0.216 t/ha, 0.163 t/ha, and 6.61% (see Fig. 6), whereas the S2 dataset yielded values of 0.234 t/ha, 0.180 t/ha, and 7.41% (see Fig. 5). Notably, these values were marginally lower using alternative algorithms compared with ANN. Additionally, DNN and XGBoost achieved high results but slightly lower than ANN. Based on this, we chose the ANN algorithm for validation.

C. Model Optimization

In the context of our RFR analysis, we evaluated the future selection of the RFR model using all VIs (see Fig. 8). Our findings revealed that the most significant values were given by

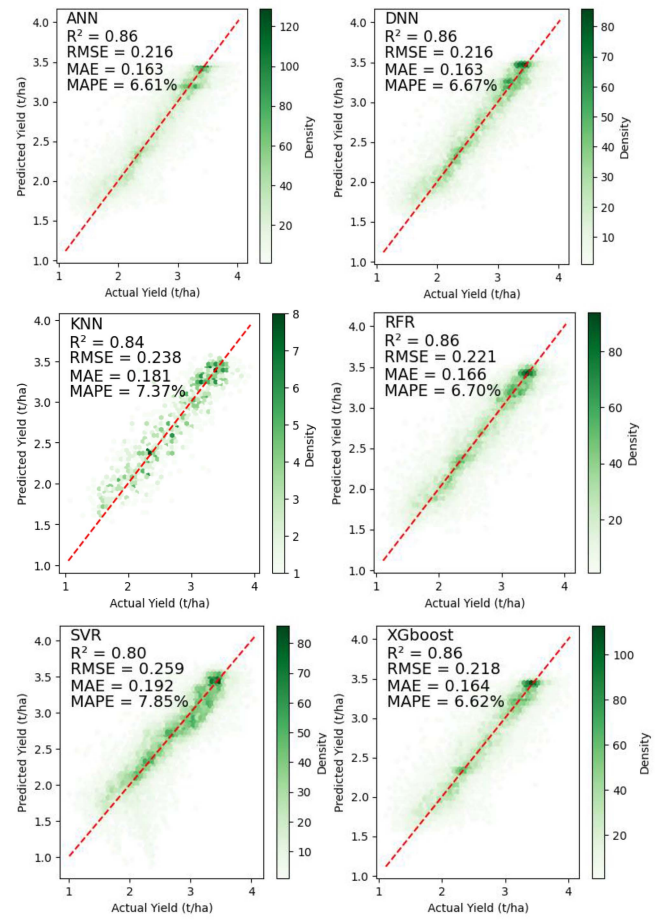


Fig. 6. Scatter plots comparing actual and predicted yields for training data, employing PS and VIs with ANN, DNN, KNN, RFR, SVR, and XGBoost.

NDVI and SAVI, with R^2 values of 0.83 and 0.82, respectively. Following closely were GNDVI at 0.79 and EVI at 0.76; the weakest correlation was observed with red edge at 0.74. Based on this, we also used the NDVI map when comparing predicted maps in Section V.

V. VALIDATION

In the validation phase, we comprehensively analyzed the ML and DL algorithms, initially focusing on a single parcel, as shown in Figs. 5–7. Subsequently, we extended our analysis to another parcel based on the best-performing algorithms. Our evaluation encompassed the generation of predicted, residual, and normalized NDVI maps for two distinct satellite images and their fused data. Particularly, our comparative analysis revealed a consistent pattern across the datasets. Specifically, the fusion data consistently outperformed both individual satellite images during crop yield prediction. As shown in Fig. 9, the predicted yield map derived from the fusion image predominantly exhibited values ranging from 1.5 to 2.5 t/ha. In contrast, the PS image yielded predictions ranging from 0.5 to 2 t/ha, and the predictions for the S2 image ranged from 0.5 to 2.0 t/ha.

Fig. 10 illustrates the residual map that shows the difference between the actual and predicted yield values. The fusion data,

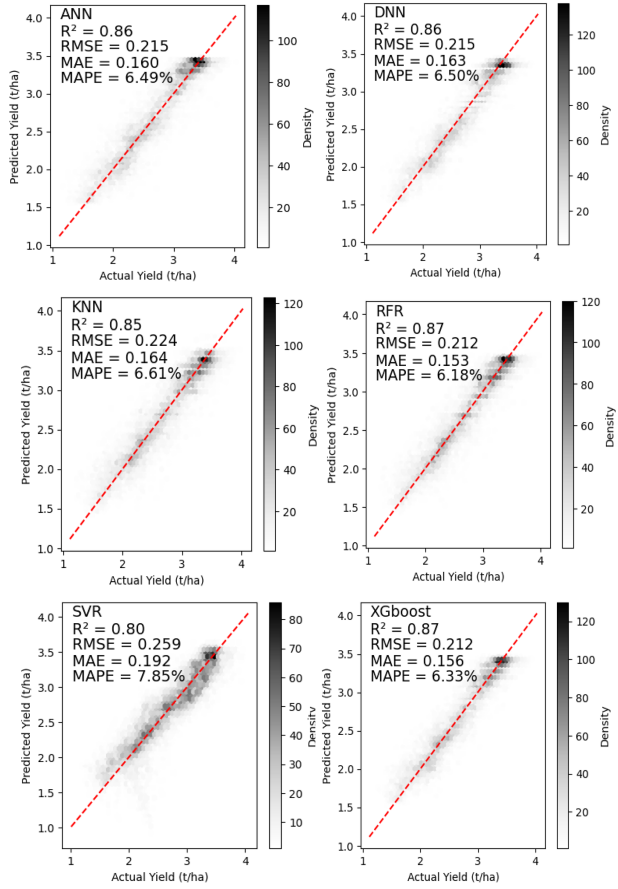


Fig. 7. Scatter plots comparing actual and predicted yields for training data, employing fusion data and VIs with ANN, DNN, KNN, RFR, SVR, and XGBoost.

when employed for yield prediction, demonstrated a relatively minor error range, with discrepancies ranging from -0.5 to 0.2 t/ha. In contrast, the PS and S2 datasets showed greater prediction errors. Our investigation extended to the analysis of NDVI maps, as shown in Fig. 11. This analysis revealed a clear correlation between NDVI values and crop productivity predictions. In regions with high predicted productivity, NDVI values were significantly higher, whereas lower NDVI values were observed in areas with lower predicted yields.

We generated boxplots for fusion, PS, and S2 data to visualize the distribution of observed and predicted crop yields as a part of model validation (see Fig. 12). The boxplots serve as model validation, visually comparing observed crop yields with their corresponding predicted values. The boxplot shows a significant correlation between the observed and predicted crop yields across all three datasets, indicating a substantial and consistent relationship.

VI. DISCUSSION

A. Time-Series Analysis of Phenology

In this study, the NDVI was computed from April to October. The phenological stages of soybean growth were identified using information from the S2 and PS satellites. Because the data



Fig. 8. Example of future selection of the VIs with random forest model.

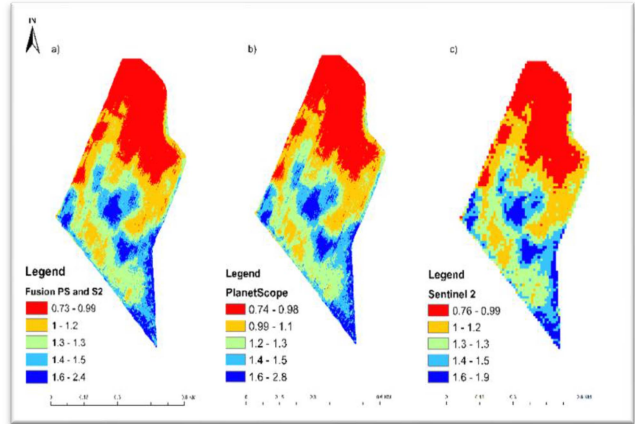


Fig. 9. Predicted crop yields of the validation field at the pixel level.

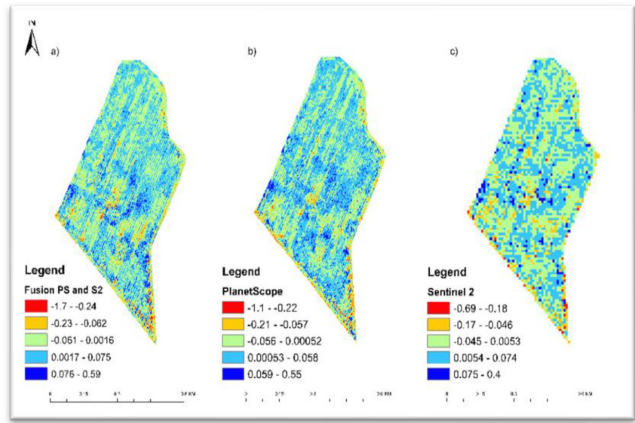


Fig. 10. Residual map: Differences between the observed and predicted yield.

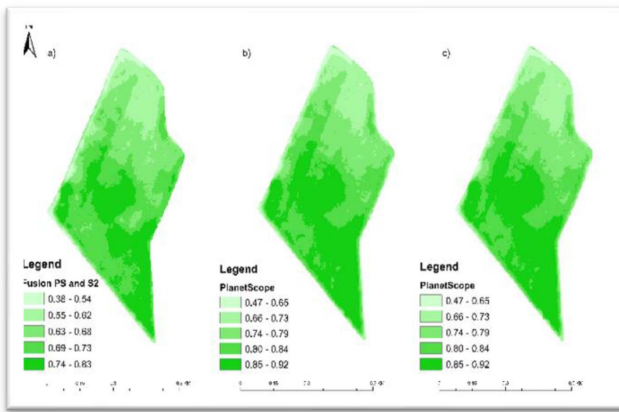


Fig. 11. NDVI map for the three datasets.

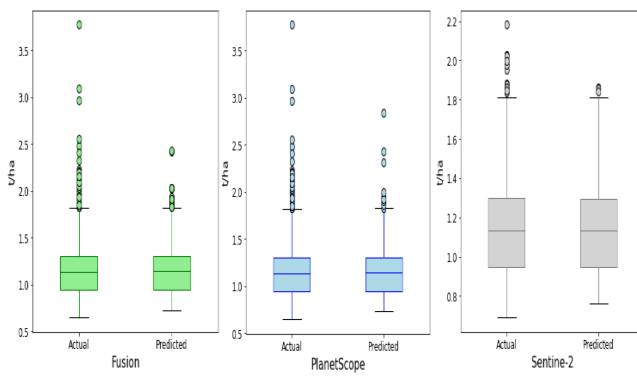


Fig. 12. Boxplots for actual and predicted yield values using the model.

were interpolated at a consistent five-day interval, temporal smoothing was accomplished, resulting in an NDVI time series that vividly demonstrates the phenological period. To ensure the integration of the two datasets, the accurate point, i.e., the beginning of August when soybean growth peaks, was specifically chosen. This result is consistent with the study by Skakun et al. [70]. This choice was based on the finding of the most important growth stages in both satellite imagery and practical feasibility. Seasonal peak VI values provide more accurate yield estimates [71], [72].

B. Advantages of ML Fused Imagery

Planet's PS satellites are known for their cost-effectiveness, providing high spatiotemporal imagery at a more economical price than conventional satellites. However, CubeSat constellations, such as PS, often grapple with challenges related to variations in radiometric quality between different sensors within the constellation and disparities in their spectral responses. These factors contribute to noise in the time-series data collected from these sensors [8], [73]. The noise in the PS data can be removed by fusing the image with a reliable and consistent dataset, such as S2, to get over this restriction [31], [33].

The fusion technique presented in this study successfully resolves the problems with PS spectral responses. As shown in Fig. 3, the outcome is the creation of images that maintain

the spectral quality of S2 while retaining the higher spatial and temporal resolution qualities of PS. This means that surface reflectance images in RGB, red edge, and NIR compatible with S2 can be produced, as well as bands compatible with PS at a high resolution of 3 m. Similar fusion methods were used in [8]; however, there was a difference in the quantity of bands used. They used four bands from PS in this method. In contrast, we used the new PS bands, which enabled us to incorporate the red-edge band. This addition made it easier to calculate the red-edge VI, setting our fusion approach apart by adding this extra spectrum data.

The proposed fusion technique makes it possible to observe plant phenological stages by creating an extensive time series of images throughout the growth cycle. Users can hypothetically integrate images from different sensors due to the robustness and flexibility of this approach. The method's adaptability is increased by the fleets of Earth observation satellites continuing to expand, enabling unprecedented spectral resolution in several bands. Remarkably, the technique is not limited by the number of bands, utilizing high spatial resolution bands to include a wider spectrum of lower resolutions. Furthermore, other researchers employing fusion imagery from satellites achieved exceptional outcomes. For instance, the grain yield predicted by the SAFY model was compared with the harvester's yield map [10]. The yield prediction accuracy of LAI, derived from the fusion of PS and S2 images, was higher ($RMSE = 69 \text{ g/m}^2$) than that of S2 LAI alone ($RMSE = 88 \text{ g/m}^2$). Meanwhile, a 2.5 m spatial resolution was used in [74], expanding the use of the process to ten S2 bands ($B_2, B_3, B_4, B_8, B_5, B_6, B_7, B_{8a}, B_{11}$, and B_{12}) with noticeably higher accuracy. The potential of DL for image fusion integrating numerous satellites and sensors will be explored in future studies. The proposed approach exhibits outstanding local spectral and spatial precision at the scale of the studied S2 tile. Each band, the major land cover, and the PS strip (i.e., individual PS satellite and orbit) are precisely defined.

C. Effectiveness of ANN for Training and Validation

First, we computed VIs for three distinct datasets: PS, S2, and fused data. Subsequently, we applied the ML and DL algorithms to the same training dataset. We assessed the performance of these algorithms using various metrics, including R^2 , RMSE, MAE, and MAPE, for RFR, SVR, KNN, XGBoost, DNN, and ANN. ANN consistently outperformed the other algorithms across all three datasets. The ANN model executed in [75] demonstrates superior performance for crop yield prediction in agriculture. Thus, we employed an ANN for the validation phase to generate predictive maps.

For the predicted maps, we generated map-based VIs. The results show that the fused predicted map outperformed the other two predicted maps, as depicted in Fig. 9. Notably, the fused predicted map displayed the highest values, with the 1.8–2 t/ha range being more prominently detected than PS and S2. Analyzing the model's residuals provides important information about the model's accuracy and fitness. Assuming that errors (residuals) have an expected value of zero, that they

are uncorrelated, and that their variance is equal, demonstrating the homoscedasticity of errors, the parameters evaluated in the residual analysis are consistent with the Gauss–Markov theorem [76]. We also evaluated them to determine whether the residuals from the two models adhered to a normal distribution. The residual map for the fused dataset in Fig. 10 reveals that the errors in the PS dataset are clustered around zero, indicating minimal deviations. In contrast, the S2 dataset exhibits slightly higher error values.

D. Comparative Analysis of Fusion Techniques

We generate another fusion technique and compare it with new fusion methods.

- 1) PyDMS is a decision-tree-based algorithm used for image sharpening or disaggregation. PyDMS takes a low-resolution image and uses information from a corresponding high-resolution image to enhance the details and resolution of the low-resolution one. PyDMS is first trained on a set of paired images—low-resolution versions and their corresponding high-resolution counterparts. During this phase, the algorithm builds a decision-tree model that learns the relationship between the low-resolution and high-resolution data. Once trained, PyDMS can be applied to any new low-resolution image. It uses the decision-tree model to predict the missing details and reconstruct a higher resolution version of the image. PyDMS can produce sharper and more accurate results compared with other methods, especially for complex images with fine details [38]. The algorithm can be easily adapted to different types of images and resolutions. It also allows for customizing the decision-tree model and adding additional features for improved performance. PyDMS is an open-source Python library, making it freely available for anyone to use and modify. This allows for further development and contributions from the community.
- 2) S2 data were first resampled to a spatial resolution of 3 m, following that a subset containing the relevant bands was produced. The field-level reflection values were retrieved for each band. The steps were to add together both bands' pixels, divide the total by 2, and then put the processed bands combined to create a fusion image [8]. The QGIS 3.16 software was used to carry out all these assignments.
- 3) Utilize the high-pass filter (HPF) resolution merge technique to integrate high-resolution panchromatic data with lower resolution multispectral data, yielding an output that exhibits both fine detail and an authentic representation of the original multispectral scene colors [77]. This functionality is an implementation of the “HP resolution merge” method, developed and proposed by Ute Gangkofner from Geoville, Inc., and Derrold Holcomb from ERDAS, Inc. The procedure entails applying a convolution with an HPF to the high-resolution data, followed by its combination with the lower resolution multispectral data. We pan sharpened the corresponding bands individually as our data are not panchromatic, and we finally merged all the bands for creating fusion dataset; the whole process was done in ERDAS 2020 software.

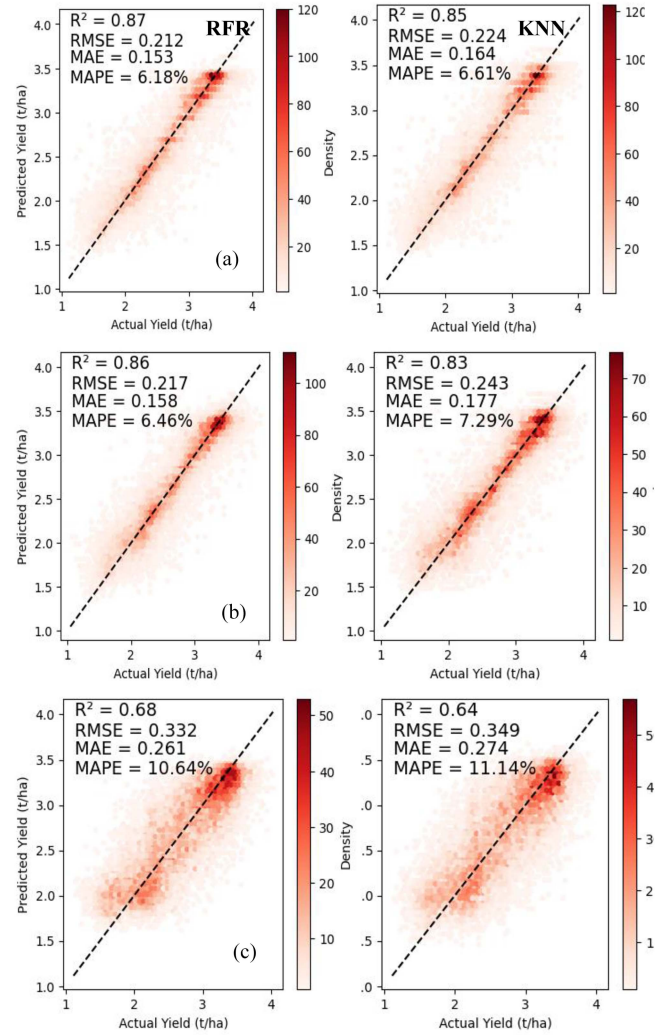


Fig. 13. Prediction of soybean yield by RFR and KNN algorithms using three different fusion techniques. (a) pyDMS fusion technique. (b) Band-to-band fusion method. (c) HPF fusion method.

Then, we predict soybean yield with two algorithms RFR and KNN for comparing all fusion techniques.

After analyzing all the fusion methods, the pyDMS fusion yielded the most favorable results, indicating its better performance in both algorithms. The outcomes are as follows in particular: R^2 values 0.87 and 0.85. The second-best performance is the band-to-band fusion method, with R^2 values of 0.86 and 0.83. In our dataset, the HPF fusion approach produced the lowest results, with R^2 values between 0.68 and 0.64. With every aspect considered, the pyDMS approach proved to be the most effective, as seen by its outstanding results on other metrics (Fig. 13).

E. ML and DL Techniques in Use

ANN Adaptability: ANN demonstrated better adaptability to the complexity of the dataset. ANNs can learn intricate patterns and relationships within data, especially when the dataset is large and exhibits nonlinear characteristics [78].

DNN Overfitting: DNNs may suffer from overfitting when dealing with complex data. The depth of the network can lead to capturing noise in the training data, reducing generalization performance.

1) *Hyperparameter Tuning. Optimized Parameters:* The superior performance of ANN could also be attributed to thorough hyperparameter tuning. Proper tuning of the learning rate, number of hidden layers, and neurons in each layer enhanced the ANNs ability to converge to an optimal solution [79].

2) *Handling Nonlinear Relationships. SVR Limitations:* SVR might struggle with capturing complex nonlinear relationships in the data. In scenarios where the relationships are highly nonlinear, ANNs or ensemble methods, such as XGBoost, may perform better [80].

3) *Model Interpretability. Interpretability Tradeoff:* While RFR and XGBoost performed well, they might sacrifice some interpretability due to their ensemble nature. The choice of ANN over DNN could be influenced by the need for a balance between performance and interpretability.

4) *Training Time and Computational Efficiency. Computational Efficiency:* The computational efficiency of ANNs, especially in training, might have been favorably compared with DNN, making them more practical for large-scale datasets.

The superior performance of ANN over DNN, RFR, KNN, SVR, and XGBoost in the study can be attributed to their adaptability to data complexity, feature sensitivity, effective handling of nonlinearity, optimized hyperparameters, and computational efficiency. These factors collectively contributed to the selection of ANN as the preferred ML/DL technique for the specific task of predicting crop yields.

F. Selection Rationale for ML and DL Techniques

The selection of ML and DL techniques for soybean yield prediction was meticulous, considering their proven effectiveness in handling agricultural datasets. Here is a concise overview of the chosen algorithms.

- 1) *RFR:* Known for versatility and robustness, RFRs ensemble learning and feature selection capabilities make it adept at capturing nonlinear relationships in complex agricultural datasets [81].
- 2) *KNN:* Despite its computational intensity, KNNs simplicity and effectiveness in regression tasks suit the dynamic and spatially correlated nature of agricultural data.
- 3) *SVR:* Selected for its ability to model complex relationships in high-dimensional spaces, SVR excels in capturing nuanced factors affecting soybean crop yields [82].
- 4) *XGBoost:* Popular for its speed, efficiency, and capacity to handle missing data, XGBoost's feature selection capabilities contribute to the accurate soybean yield predictions [83].
- 5) *DNN and ANN:* Chosen for their prowess in capturing intricate, nonlinear relationships, the multilayered architectures of DNN and ANN prove valuable in representing complex patterns for soybean yield prediction [84]. The decision to employ these techniques was well founded, considering their strengths and track records in similar

studies. Comprehensive performance evaluations indicated that ANN consistently outperformed other methods, justifying its preference as the primary method for soybean yield prediction in this study.

G. Limitations

One of the limitations of this study is that we employed phenological data to fuse data from only one day. However, we intend to create a time series in our subsequent research. Fusion methods may face challenges in achieving perfect spatial and spectral alignment between PS and S2 data, leading to discrepancies in the fused datasets. There are two challenges in current image fusion approaches, as identified in [85]. First, these methods commonly presume short time intervals between images, a condition not always met in large-scale high-resolution images and numerous real-world scenarios. Second, the potential spectral misalignment between multispectral and RGB images can lead to spectral distortions in S2 imagery during the fusion process. Although S2 data can be used for free, PS data application is not free. However, even if the results are positive, it could be difficult for farmers to predict future agricultural crops. To further improve agricultural convenience, the same method will be used in the future for forecasting other crop types using either Sentinel-1 and S2 or Landsat data.

VII. CONCLUSION

In this study, we fused S2 data with the new PS eight-band data to predict soybean production and compared each prediction. The findings showed that the fusion data from 1.5 to 2.5 tons were mainly responsible for the yield prediction from fusion with higher values and fewer errors. For PS data, it was between 0.5 and 2 t/ha, whereas it was between 0.5 and 2.0 t/ha for S2. We also used Vis for the evaluation of the models. In the validation phase, we compared crop prediction using an NDVI map. This study demonstrated the effectiveness of ANN in predicting crop yields, outperforming other algorithms across diverse datasets. The fusion of PS and S2 data is advantageous because it enhances spatial and temporal resolution while maintaining spectral quality. Model validation demonstrated the superior performance of the fusion dataset in predicting crop yields compared with individual satellite images. This study provides valuable insights into phenology monitoring, image fusion accuracy, and the effectiveness of ML algorithms in predicting crop yields, emphasizing the benefits of fused imagery.

Although S2 and PS data integration has proven effective for crop prediction, the new fusion method expands its use to combine several image sources with different spectral, spatial, and temporal resolutions. This novel fusion method's adaptability makes it possible to monitor crops broadly and continuously on a daily basis at high resolution on a wide scale. In addition to crop prediction, it offers potential opportunities for precision agriculture. This fusion technique is essential for monitoring crop health and growth, improving agricultural practices, such as fertilization and water management, and improving yield forecast accuracy.

ACKNOWLEDGMENT

The authors would like to thank ESA for the availability of Sentinel-2 MSI at the Copernicus Open Access Hub and R software developers for such a powerful program. Sunflower yield data and phenological stages were collected at small-scale farmlands in collaboration with local farmers.

REFERENCES

- [1] A. Nyéki, A. J. Kovács, M. Neményi, and G. Milics, "Conference report from 13th European conference on precision agriculture (ECPA)," *Environ. Sci. Europe*, vol. 33, no. 1, Dec. 2021, Art. no. 116, doi: [10.1186/s12302-021-00559-y](https://doi.org/10.1186/s12302-021-00559-y).
- [2] S. Mourtzinis, F. J. Arriaga, K. S. Balkcom, and B. V. Ortiz, "Corn grain and stover yield prediction at R1 growth stage," *Agron. J.*, vol. 105, no. 4, pp. 1045–1050, Jul. 2013, doi: [10.2134/agronj2012.0393](https://doi.org/10.2134/agronj2012.0393).
- [3] M. Schut, J.-J. Cadilhon, M. Misiko, and I. Dror, "Do mature innovation platforms make a difference in agricultural research for development? A meta-analysis of case studies," *Exp. Agriculture*, vol. 54, no. 1, pp. 96–119, 2018.
- [4] S. Wolfert, L. Ge, C. Verdouw, and M.-J. Bogaardt, "Big data in smart farming—A review," *Agricultural Syst.*, vol. 153, pp. 69–80, May 2017, doi: [10.1016/j.agysy.2017.01.023](https://doi.org/10.1016/j.agysy.2017.01.023).
- [5] D. Radočaj, M. Jurišić, M. Gašparović, and I. Plaščák, "Optimal soybean (*glycine max* L.) land suitability using GIS-based multicriteria analysis and Sentinel-2 multitemporal images," *Remote Sens.*, vol. 12, no. 9, May 2020, Art. no. 1463, doi: [10.3390/rs12091463](https://doi.org/10.3390/rs12091463).
- [6] L. Zhong, L. Hu, and H. Zhou, "Deep learning based multi-temporal crop classification," *Remote Sens. Environ.*, vol. 221, pp. 430–443, Feb. 2019, doi: [10.1016/j.rse.2018.11.032](https://doi.org/10.1016/j.rse.2018.11.032).
- [7] D. Helman et al., "Using time series of high-resolution planet satellite images to monitor grapevine stem water potential in commercial vineyards," *Remote Sens.*, vol. 10, no. 10, Oct. 2018, Art. no. 1615, doi: [10.3390/rs10101615](https://doi.org/10.3390/rs10101615).
- [8] Y. Sadeh et al., "Fusion of Sentinel-2 and PlanetScope time-series data into daily 3 m surface reflectance and wheat LAI monitoring," *Int. J. Appl. Earth Observ. Geoinf.*, vol. 96, Apr. 2021, Art. no. 102260, doi: [10.1016/j.jag.2020.102260](https://doi.org/10.1016/j.jag.2020.102260).
- [9] A. Y. Cho, S.-E. Park, D.-J. Kim, J. Kim, C. Li, and J. Song, "Burned area mapping using unitemporal PlanetScope imagery with a deep learning based approach," *IEEE J. Sel. Topics Appl. Earth Observ. Remote Sens.*, vol. 16, pp. 242–253, Jan. 2023, doi: [10.1109/JSTARS.2022.3225070](https://doi.org/10.1109/JSTARS.2022.3225070).
- [10] V. S. Manivasagam, Y. Sadeh, G. Kaplan, D. J. Bonfil, and O. Rozenstein, "Studying the feasibility of assimilating Sentinel-2 and PlanetScope imagery into the SAFY crop model to predict within-field wheat yield," *Remote Sens.*, vol. 13, no. 12, Jun. 2021, Art. no. 2395, doi: [10.3390/rs13122395](https://doi.org/10.3390/rs13122395).
- [11] Y. Sun, B. Xue, M. Zhang, and G. G. Yen, "Completely automated CNN architecture design based on blocks," *IEEE Trans. Neural Netw. Learn. Syst.*, vol. 31, no. 4, pp. 1242–1254, Apr. 2020.
- [12] D. B. Lobell, J. I. Ortiz-Monasterio, G. P. Asner, P. A. Matson, R. L. Naylor, and W. P. Falcon, "Analysis of wheat yield and climatic trends in Mexico," *Field Crops Res.*, vol. 94, no. 2/3, pp. 250–256, Nov. 2005, doi: [10.1016/j.fcr.2005.01.007](https://doi.org/10.1016/j.fcr.2005.01.007).
- [13] A. Magri, H. M. Van Es, M. A. Glos, and W. J. Cox, "Soil test, aerial image and yield data as inputs for site-specific fertility and hybrid management under maize," *Precis. Agriculture*, vol. 6, pp. 87–110, 2005.
- [14] G. Tan and R. Shibasaki, "Global estimation of crop productivity and the impacts of global warming by GIS and EPIC integration," *Ecol. Model.*, vol. 168, no. 3, pp. 357–370, Oct. 2003, doi: [10.1016/S0304-3800\(03\)00146-7](https://doi.org/10.1016/S0304-3800(03)00146-7).
- [15] J. Lofton, B. S. Tubana, Y. Kanke, J. Teboh, H. Viator, and M. Dalen, "Estimating sugarcane yield potential using an in-season determination of normalized difference vegetative index," *Sensors*, vol. 12, no. 6, pp. 7529–7547, 2012.
- [16] R. Shrestha, L. Di, G. Y. Eugene, L. Kang, Y. Shao, and Y. Bai, "Regression model to estimate flood impact on corn yield using MODIS NDVI and USDA cropland data layer," *J. Integrative Agriculture*, vol. 16, no. 2, pp. 398–407, 2017.
- [17] B. Yu and S. Shang, "Multi-year mapping of major crop yields in an irrigation district from high spatial and temporal resolution vegetation index," *Sensors*, vol. 18, no. 11, 2018, Art. no. 3787.
- [18] S. S. Panda, D. P. Ames, and S. Panigrahi, "Application of vegetation indices for agricultural crop yield prediction using neural network techniques," *Remote Sens.*, vol. 2, no. 3, pp. 673–696, Mar. 2010, doi: [10.3390/rs2030673](https://doi.org/10.3390/rs2030673).
- [19] J. Xue and B. Su, "Significant remote sensing vegetation indices: A review of developments and applications," *J. Sensors*, vol. 2017, 2017, Art. no. 1353691, doi: [10.1155/2017/1353691](https://doi.org/10.1155/2017/1353691).
- [20] S. Nebiker, N. Lack, M. Abächerli, and S. Läderach, "Light-weight multispectral UAV sensors and their capabilities for predicting grain yield and detecting plant diseases," *Int. Arch. Photogramm., Remote Sens. Spatial Inf. Sci.*, vol. 41, pp. 963–970, 2016.
- [21] B. Ji, Y. Sun, S. Yang, and J. Wan, "Artificial neural networks for rice yield prediction in mountainous regions," *J. Agricultural Sci.*, vol. 145, no. 3, pp. 249–261, 2007.
- [22] R. Nathan and H. C. Muller-Landau, "Spatial patterns of seed dispersal, their determinants and consequences for recruitment," *Trends Ecol. Evol.*, vol. 15, no. 7, pp. 278–285, Jul. 2000, doi: [10.1016/S0169-5347\(00\)01874-7](https://doi.org/10.1016/S0169-5347(00)01874-7).
- [23] J. E. Sheehy, P. L. Mitchell, and A. B. Ferrer, "Decline in rice grain yields with temperature: Models and correlations can give different estimates," *Field Crops Res.*, vol. 98, no. 2/3, pp. 151–156, 2006.
- [24] P. Rischbeck, S. Elsayed, B. Mistele, G. Barmeier, K. Heil, and U. Schmidhalter, "Data fusion of spectral, thermal and canopy height parameters for improved yield prediction of drought stressed spring barley," *Eur. J. Agronomy*, vol. 78, pp. 44–59, 2016.
- [25] A. Okonomidis, C. Catal, and A. Kassahun, "Hybrid deep learning-based models for crop yield prediction," *Appl. Artif. Intell.*, vol. 36, no. 1, 2022, Art. no. 2031822.
- [26] R. Fernandez-Beltran, T. Baidar, J. Kang, and F. Pla, "Rice-yield prediction with multi-temporal Sentinel-2 data and 3D CNN: A case study in Nepal," *Remote Sens.*, vol. 13, no. 7, 2021, Art. no. 1391.
- [27] H. Russello, "Convolutional neural networks for crop yield prediction using satellite images," *IBM Center Adv. Stud.*, 2018.
- [28] T. Van Klompenburg, A. Kassahun, and C. Catal, "Crop yield prediction using machine learning: A systematic literature review," *Comput. Electron. Agriculture*, vol. 177, Oct. 2020, Art. no. 105709, doi: [10.1016/j.compag.2020.105709](https://doi.org/10.1016/j.compag.2020.105709).
- [29] Y. LeCun and Y. Bengio, "Convolutional networks for images, speech, and time series," in *The Handbook of Brain Theory and Neural Networks*. Cambridge, MA, USA: MIT Press, 1998, pp. 255–258.
- [30] H. Kimm et al., "Deriving high-spatiotemporal-resolution leaf area index for agroecosystems in the U.S. corn belt using planet labs CubeSat and STAIR fusion data," *Remote Sens. Environ.*, vol. 239, Mar. 2020, Art. no. 111615, doi: [10.1016/j.rse.2019.111615](https://doi.org/10.1016/j.rse.2019.111615).
- [31] Y. Luo, K. Guan, and J. Peng, "STAIR: A generic and fully-automated method to fuse multiple sources of optical satellite data to generate a high-resolution, daily and cloud-/gap-free surface reflectance product," *Remote Sens. Environ.*, vol. 214, pp. 87–99, Sep. 2018, doi: [10.1016/j.rse.2018.04.042](https://doi.org/10.1016/j.rse.2018.04.042).
- [32] M. Maimaitijiang, V. Sagan, P. Sidike, S. Hartling, F. Esposito, and F. B. Fritschi, "Soybean yield prediction from UAV using multimodal data fusion and deep learning," *Remote Sens. Environ.*, vol. 237, Feb. 2020, Art. no. 111599, doi: [10.1016/j.rse.2019.111599](https://doi.org/10.1016/j.rse.2019.111599).
- [33] T. G. Andrade, A. S. D. Andrade Junior, M. O. Souza, J. W. B. Lopes, and P. F. D. M. J. Vieira, "Soybean yield prediction using remote sensing in Southwestern Piauí State, Brazil," *Rev. Caatinga*, vol. 35, no. 1, pp. 105–116, Mar. 2022, doi: [10.1590/1983-21252022v35n11rc](https://doi.org/10.1590/1983-21252022v35n11rc).
- [34] G. Lyle, B. A. Bryan, and B. Ostendorf, "Post-processing methods to eliminate erroneous grain yield measurements: Review and directions for future development," *Precis. Agriculture*, vol. 15, pp. 377–402, 2014.
- [35] D. Vijayasekaran, "Sen2-agri—Crop type mapping pilot study using Sentinel-2 satellite imagery in India," *Int. Arch. Photogramm., Remote Sens. Spatial Inf. Sci.*, vol. XLII-3/W6, pp. 175–180, Jul. 2019, doi: [10.5194/isprs-archives-XLII-3-W6-175-2019](https://doi.org/10.5194/isprs-archives-XLII-3-W6-175-2019).
- [36] F. Gao, W. Kustas, and M. Anderson, "A data mining approach for sharpening thermal satellite imagery over land," *Remote Sens.*, vol. 4, no. 11, pp. 3287–3319, Oct. 2012, doi: [10.3390/rs4113287](https://doi.org/10.3390/rs4113287).
- [37] L. Breiman, "Random forests," *Mach. Learn.*, vol. 45, no. 1, pp. 5–32, 2001, doi: [10.1023/A:1010933404324](https://doi.org/10.1023/A:1010933404324).
- [38] J. W. Rouse, R. H. Haas, J. A. Schell, and D. W. Deering, "Monitoring vegetation systems in the great plains with ERTS," *NASA Special Publ.*, vol. 351, no. 1, 1974, Art. no. 309.
- [39] A. A. Gitelson, Y. J. Kaufman, and M. N. Merzlyak, "Use of a green channel in remote sensing of global vegetation from EOS-MODIS," *Remote Sens. Environ.*, vol. 58, no. 3, pp. 289–298, 1996.

- [40] L. J. Thompson et al., "Model and sensor-based recommendation approaches for in-season nitrogen management in corn," *Agron. J.*, vol. 107, no. 6, pp. 2020–2030, Nov. 2015, doi: [10.2134/agronj15.0116](https://doi.org/10.2134/agronj15.0116).
- [41] A. V. Rocha and G. R. Shaver, "Advantages of a two band EVI calculated from solar and photosynthetically active radiation fluxes," *Agricultural Forest Meteorol.*, vol. 149, no. 9, pp. 1560–1563, Sep. 2009, doi: [10.1016/j.agrformet.2009.03.016](https://doi.org/10.1016/j.agrformet.2009.03.016).
- [42] A. R. Huete, "A soil-adjusted vegetation index (SAVI)," *Remote Sens. Environ.*, vol. 25, no. 3, pp. 295–309, Aug. 1988, doi: [10.1016/0034-4257\(88\)90106-X](https://doi.org/10.1016/0034-4257(88)90106-X).
- [43] A. A. Gitelson, Y. Peng, and K. F. Huemmrich, "Relationship between fraction of radiation absorbed by photosynthesizing maize and soybean canopies and NDVI from remotely sensed data taken at close range and from MODIS 250m resolution data," *Remote Sens. Environ.*, vol. 147, pp. 108–120, May 2014, doi: [10.1016/j.rse.2014.02.014](https://doi.org/10.1016/j.rse.2014.02.014).
- [44] C. J. Tucker, "Red and photographic infrared linear combinations for monitoring vegetation," *Remote Sens. Environ.*, vol. 8, no. 2, pp. 127–150, 1979.
- [45] C. J. Tucker and P. J. Sellers, "Satellite remote sensing of primary production," *Int. J. Remote Sens.*, vol. 7, no. 11, pp. 1395–1416, 1986.
- [46] J. F. Shanahan et al., "Use of remote-sensing imagery to estimate corn grain yield," *Agronomy J.*, vol. 93, no. 3, pp. 583–589, 2001.
- [47] T. J. Jackson et al., "Vegetation water content mapping using Landsat data derived normalized difference water index for corn and soybeans," *Remote Sens. Environ.*, vol. 92, no. 4, pp. 475–482, 2004.
- [48] P. Defourny et al., "Near real-time agriculture monitoring at national scale at parcel resolution: Performance assessment of the Sen2-Agri automated system in various cropping systems around the world," *Remote Sens. Environ.*, vol. 221, pp. 551–568, Feb. 2019, doi: [10.1016/j.rse.2018.11.007](https://doi.org/10.1016/j.rse.2018.11.007).
- [49] D. Giamelle, L. Vescovo, and F. Mason, "Estimation of grassland biophysical parameters using hyperspectral reflectance for fire risk map prediction," *Int. J. Wildland Fire*, vol. 18, no. 7, pp. 815–824, 2009.
- [50] S. J. Muller, P. Sithole, A. Singels, and A. Van Niekerk, "Assessing the fidelity of Landsat-based fAPAR models in two diverse sugarcane growing regions," *Comput. Electron. Agriculture*, vol. 170, Mar. 2020, Art. no. 105248, doi: [10.1016/j.compag.2020.105248](https://doi.org/10.1016/j.compag.2020.105248).
- [51] M. Rumli and T. Vulic, "Importance of phenological observations and predictions in agriculture," *J. Agricultural Sci.*, vol. 50, no. 2, pp. 217–225, 2005, doi: [10.2298/JAS0502217R](https://doi.org/10.2298/JAS0502217R).
- [52] N. Farmonov et al., "Combining PlanetScope and Sentinel-2 images with environmental data for improved wheat yield estimation," *Int. J. Digit. Earth*, vol. 16, no. 1, pp. 847–867, Dec. 2023, doi: [10.1080/17538947.2023.2186505](https://doi.org/10.1080/17538947.2023.2186505).
- [53] Z. Liu et al., "Winter wheat yield estimation based on assimilated Sentinel-2 images with the CERES-wheat model," *J. Integrative Agriculture*, vol. 20, no. 7, pp. 1958–1968, Jul. 2021, doi: [10.1016/S2095-3119\(20\)63489-9](https://doi.org/10.1016/S2095-3119(20)63489-9).
- [54] S. Mopidevi, V. Singitham, B. Thippani, R. Shanthula, and N. S. P. Vallabhaneni, "Plant growth and yield prediction using ML and DL algorithms," in *Proc. Int. Conf. Electron. Renewable Syst.*, 2022, pp. 1470–1477, doi: [10.1109/ICEARS53579.2022.9751906](https://doi.org/10.1109/ICEARS53579.2022.9751906).
- [55] P. F. Smith, S. Ganesh, and P. Liu, "A comparison of random forest regression and multiple linear regression for prediction in neuroscience," *J. Neurosci. Methods*, vol. 220, no. 1, pp. 85–91, Oct. 2013, doi: [10.1016/j.jneumeth.2013.08.024](https://doi.org/10.1016/j.jneumeth.2013.08.024).
- [56] S. Cvejić et al., "Oil yield prediction for sunflower hybrid selection using different machine learning algorithms," *Sci. Rep.*, vol. 13, no. 1, Oct. 2023, Art. no. 17611, doi: [10.1038/s41598-023-44993](https://doi.org/10.1038/s41598-023-44993).
- [57] R. Medar, V. S. Rajpurohit, and S. Shweta, "Crop yield prediction using machine learning techniques," in *Proc. IEEE 5th Int. Conf. Convergence Technol.*, 2019, pp. 1–5, doi: [10.1109/I2CT45611.2019.9033611](https://doi.org/10.1109/I2CT45611.2019.9033611).
- [58] D. Basak, S. Pal, and D. C. Patranabis, "Support vector regression," *Neural Inf. Process. – Letters Rev.*, vol. 11, no. 10, pp. 203–213, Oct. 2007.
- [59] A. Dezhkam and M. T. Manzuri, "Forecasting stock market for an efficient portfolio by combining XGBoost and Hilbert-Huang transform," *Eng. Appl. Artif. Intell.*, vol. 118, Feb. 2023, Art. no. 105626, doi: [10.1016/j.engappai.2022.105626](https://doi.org/10.1016/j.engappai.2022.105626).
- [60] L. Yang and A. Shami, "On hyperparameter optimization of machine learning algorithms: Theory and practice," *Neurocomputing*, vol. 415, pp. 295–316, Nov. 2020, doi: [10.1016/j.neucom.2020.07.061](https://doi.org/10.1016/j.neucom.2020.07.061).
- [61] Y. Kang, M. Ozdogan, X. Zhu, Z. Ye, C. Hain, and M. Anderson, "Comparative assessment of environmental variables and machine learning algorithms for maize yield prediction in the US midwest," *Environ. Res. Lett.*, vol. 15, no. 6, Jun. 2020, Art. no. 064005, doi: [10.1088/1748-9326/ab7d9](https://doi.org/10.1088/1748-9326/ab7d9).
- [62] A. Nigam, S. Garg, A. Agrawal, and P. Agrawal, "Crop yield prediction using machine learning algorithms," in *Proc. 5th Int. Conf. Image Inf. Process.*, 2019, pp. 125–130, doi: [10.1109/ICIIP47207.2019.8985951](https://doi.org/10.1109/ICIIP47207.2019.8985951).
- [63] M. Shahhosseini, R. A. Martinez-Feria, G. Hu, and S. V. Archontoulis, "Maize yield and nitrate loss prediction with machine learning algorithms," *Environ. Res. Lett.*, vol. 14, no. 12, Dec. 2019, Art. no. 124026, doi: [10.1088/1748-9326/ab5268](https://doi.org/10.1088/1748-9326/ab5268).
- [64] I. Goodfellow, Y. Bengio, and A. Courville, *Deep Learning*. Cambridge, MA, USA: MIT Press, 2016.
- [65] W. Liu, Z. Wang, X. Liu, N. Zeng, Y. Liu, and F. E. Alsaadi, "A survey of deep neural network architectures and their applications," *Neurocomputing*, vol. 234, pp. 11–26, Apr. 2017, doi: [10.1016/j.neucom.2016.12.038](https://doi.org/10.1016/j.neucom.2016.12.038).
- [66] S. Khaki, Z. Khalilzadeh, and L. Wang, "Predicting yield performance of parents in plant breeding: A neural collaborative filtering approach," *PLoS One*, vol. 15, no. 5, May 2020, Art. no. e0233382, doi: [10.1371/journal.pone.0233382](https://doi.org/10.1371/journal.pone.0233382).
- [67] S. Khaki and L. Wang, "Crop yield prediction using deep neural networks," *Front. Plant Sci.*, vol. 10, May 2019, Art. no. 621, doi: [10.3389/fpls.2019.00621](https://doi.org/10.3389/fpls.2019.00621).
- [68] S.-C. Wang, "Artificial neural network," in *Interdisciplinary Computing in Java Programming*. Berlin, Germany: Springer, 2003, pp. 81–100, doi: [10.1007/978-1-4615-0377-4_5](https://doi.org/10.1007/978-1-4615-0377-4_5).
- [69] O. Adisa et al., "Application of artificial neural network for predicting maize production in South Africa," *Sustainability*, vol. 11, no. 4, Feb. 2019, Art. no. 1145, doi: [10.3390/su11041145](https://doi.org/10.3390/su11041145).
- [70] S. Skakun et al., "Assessing within-field corn and soybean yield variability from WorldView-3, planet, Sentinel-2, and Landsat 8 satellite imagery," *Remote Sens.*, vol. 13, no. 5, Feb. 2021, Art. no. 872, doi: [10.3390/rs13050872](https://doi.org/10.3390/rs13050872).
- [71] K. Amankulova, N. Farmonov, and L. Mucsi, "Time-series analysis of Sentinel-2 satellite images for sunflower yield estimation," *Smart Agricultural Technol.*, vol. 3, Feb. 2023, Art. no. 100098, doi: [10.1016/j.jatech.2022.100098](https://doi.org/10.1016/j.jatech.2022.100098).
- [72] C. Li et al., "Maize yield estimation in intercropped smallholder fields using satellite data in Southern Malawi," *Remote Sens.*, vol. 14, no. 10, May 2022, Art. no. 2458, doi: [10.3390/rs14102458](https://doi.org/10.3390/rs14102458).
- [73] R. Houborg and M. F. McCabe, "Daily retrieval of NDVI and LAI at 3 m resolution via the fusion of CubeSat, Landsat, and MODIS data," *Remote Sens.*, vol. 10, no. 6, Jun. 2018, Art. no. 890, doi: [10.3390/rs10060890](https://doi.org/10.3390/rs10060890).
- [74] N. Latte and P. Lejeune, "PlanetScope radiometric normalization and Sentinel-2 super-resolution (2.5 m): A straightforward spectral-spatial fusion of multi-satellite multi-sensor images using residual convolutional neural networks," *Remote Sens.*, vol. 12, no. 15, Jul. 2020, Art. no. 2366, doi: [10.3390/rs12152366](https://doi.org/10.3390/rs12152366).
- [75] M. S. Basir, M. Chowdhury, M. N. Islam, and M. Ashik-E-Rabbani, "Artificial neural network model in predicting yield of mechanically transplanted rice from transplanting parameters in Bangladesh," *J. Agriculture Food Res.*, vol. 5, Sep. 2021, Art. no. 100186, doi: [10.1016/j.jafr.2021.100186](https://doi.org/10.1016/j.jafr.2021.100186).
- [76] K. Chu, *Principles of Econometrics*. Hoboken, NJ, USA: Wiley, 1971.
- [77] S. Dahiya, P. K. Garg, and M. K. Jat, "A comparative study of various pixel-based image fusion techniques as applied to an urban environment," *Int. J. Image Data Fusion*, vol. 4, no. 3, pp. 197–213, Sep. 2013, doi: [10.1080/19479832.2013.778335](https://doi.org/10.1080/19479832.2013.778335).
- [78] D. C. Mocanu, E. Mocanu, P. Stone, P. H. Nguyen, M. Gibescu, and A. Liotta, "Scalable training of artificial neural networks with adaptive sparse connectivity inspired by network science," *Nature Commun.*, vol. 9, no. 1, Jun. 2018, Art. no. 2383, doi: [10.1038/s41467-018-04316-3](https://doi.org/10.1038/s41467-018-04316-3).
- [79] N. Bacanin, T. Bezdan, E. Tuba, I. Strumberger, and M. Tuba, "Optimizing convolutional neural network hyperparameters by enhanced swarm intelligence metaheuristics," *Algorithms*, vol. 13, no. 3, Mar. 2020, Art. no. 67, doi: [10.3390/a13030067](https://doi.org/10.3390/a13030067).
- [80] S. Wickramanayake and H. M. N. Bandara, "Fuel consumption prediction of fleet vehicles using machine learning: A comparative study," in *Proc. Moratuwa Eng. Res. Conf.*, 2016, pp. 90–95.
- [81] Q. Li, S. Xu, J. Zhuang, J. Liu, Y. Zhou, and Z. Zhang, "Ensemble learning prediction of soybean yields in China based on meteorological data," *J. Integrative Agriculture*, vol. 22, no. 6, pp. 1909–1927, Jun. 2023, doi: [10.1016/j.jia.2023.02.011](https://doi.org/10.1016/j.jia.2023.02.011).
- [82] V. B. D. Santos, A. M. F. D. Santos, J. R. D. S. C. D. Moraes, I. C. D. O. Vieira, and G. D. S. Rolim, "Machine learning algorithms for soybean yield forecasting in the Brazilian Cerrado," *J. Sci. Food Agriculture*, vol. 102, no. 9, pp. 3665–3672, Jul. 2022, doi: [10.1002/jsfa.11713](https://doi.org/10.1002/jsfa.11713).
- [83] L. Hollard, A. Durigon, and L. A. Steffelen, "Machine learning forecast of soybean yields on South Brazil," in *Ambient Intelligence and Smart Environments*, H. H. A. Valera and M. Luštrek, Eds. Amsterdam, The Netherlands: IOS Press, 2022, doi: [10.3233/AISE220028](https://doi.org/10.3233/AISE220028).
- [84] S. Yadulla, S. V. Yasa, and N. Pothu, "A deep learning model for soybean yield prediction," EasyChair, 2023. [Online]. Available: <https://easychair.org/preprints/10612>

- [85] R. Dong et al., "An adaptive image fusion method for Sentinel-2 images and high-resolution images with long-time intervals," *Int. J. Appl. Earth Observ. Geoinf.*, vol. 121, Jul. 2023, Art. no. 103381, doi: [10.1016/j.jag.2023.103381](https://doi.org/10.1016/j.jag.2023.103381).



Khilola Amankulova received the B.S. degree in land management and land cadastre from the Department of Land Use and Land Cadastre, Tashkent Institute of Irrigation and Agricultural Mechanization Engineers, Tashkent, Uzbekistan, in 2018, and the M.S. degree in geodesy and geoinformations from the Department of Geodesy and Geoinformatics, Tashkent Institute of Irrigation and Agricultural Mechanization Engineers, Tashkent, Uzbekistan. She is currently working toward the Ph.D. degree in remote sensing and geo-information for crop yield prediction with the Department of Geoinformatics, Physical and Environmental Geography, University of Szeged, Szeged, Hungary.

Her research focuses on remote sensing, precision agriculture, and goinformatics.



Nizom Farmonov received the B.S. degree in land management and land cadastre from the Department of Land Use and Land Cadastre, Tashkent Institute of Irrigation and Agricultural Mechanization Engineers, Bukhara branch, Uzbekistan, in 2018, and the M.S. degree in geodesy and geoinformations from the Department of Geodesy and Geoinformatics, Tashkent Institute of Irrigation and Agricultural Mechanization Engineers, Tashkent, Uzbekistan, in 2020. He is currently working toward the Ph.D. degree with the Department of Geoinformatics, Physical and Environmental Geography, University of Szeged, Szeged, Hungary.

His research interests include remote sensing, GIS, and crop yield forecasting with machine learning using high spatial-temporal multisource satellite data.



Enas Abdelsamei received the bachelor's and master's degrees in geophysics from the Faculty of Science, Minia University, Minya, Egypt, in 2012 and 2018, respectively. She is currently working toward the Ph.D. degree with the Department of Geoinformatics, Physical and Environmental Geography, University of Szeged, Szeged, Hungary.

She works as an Associate Researcher with Geomagnetic and Geoelectric Department, National Research Institute of Astronomy and Geophysics, Cairo, Egypt. Her research focuses on applying geophysics in road assessment, archaeology, groundwater exploration, ore deposits, and assessment of geothermal resources.



József Szatmári received the Ph.D. degree in Earth sciences from the University of Szeged, Szeged, Hungary, in 2007.

He is currently a Professor (Associate) with the Department of Geoinformatics, Physical and Environmental Geography, University of Szeged. His current research activities include modeling of environmental geographic processes production, automated processing, and areas of application of small- and medium-format aerial photographs.



Waleed Khan received the B.Sc. degree in electrical and computer engineering from COMSATS Islamabad, Abbottabad Campus, Abbottabad, Pakistan, and the M.Sc. and Ph.D. degrees in computer systems engineering from the University of Engineering and Technology, Peshawar, Pakistan.

His research interests include computer engineering and he has a keen interest in various areas, including remote sensing, deep learning, computer vision, and multimedia processing.



Mohamed Zhran received the M.S. and Ph.D. degrees from Public Works Engineering, Faculty of Engineering, Mansoura University, Mansoura, Egypt, in 2015 and 2019, respectively.

He is currently an Assistant Professor with Mansoura University, Mansoura, Egypt. His research interests include the areas of geomatics, geodesy, GNSS, GNSS radio occultation, remote sensing, and geoinformatics.



Jamshid Rustamov received the bachelor's degree from the Karshi Institute of Economics, in 2007, and the master's degree from the Tashkent Institute of Irrigation and Melioration, Tashkent, Uzbekistan, in 2009, both in land management and cadastre.

He is currently working as a Research Assistant with the Department of Land Resources Management, Karshi Institute of Irrigation and Agrotechnologies, Karshi, Uzbekistan. His research focuses on improving agricultural land management methods using advanced technologies.



Sharifboy Akhmedov received the bachelor's degree in hydromechanics from Tashkent State University, Tashkent, Uzbekistan, in 1979, the diploma with the title of specialist in technical sciences in "reclamation and agricultural mechanization," in 1992, and the Ph.D. degree from the Department of Mechanics, Bukhara Institute of Food and Light Industry Technologies, Bukhara, Uzbekistan, in 1995.

He currently works with the "TIIAME" NRU Bukhara Institute of Natural Resources Management, Bukhara, Uzbekistan.



Maksudxon Sarimsakov received the Ph.D. degree in agricultural sciences from the Uzbek Research Institute of Cotton Growing, in 1998.

He currently holds the position of Doctor of agricultural sciences, a Professor, and the Head of the Department of Water Supply and Irrigation Technologies, National Research University, "Tashkent Institute of Irrigation and Agricultural Mechanization Engineers," Tashkent, Uzbekistan, and the Institute for Managing Natural Resources, Bukhara, Uzbekistan. His scientific work focuses on the scientific and practical foundations of water-saving technologies for irrigating intensive fruit plantations in the irrigated area of Uzbekistan.



László Mucsi received the Ph.D. degree in Earth sciences from the University of Szeged, Szeged, Hungary, in 1997.

He is a Professor (Associate) with the Department of Geoinformatics, Physical and Environmental Geography, University of Szeged. His current research activities include remote sensing, time-series analysis, image classification, and artificial intelligence.